

Iris Matching Based on a Stack like Structure Graph Approach

Roushdi Mohamed FAROUK^{1,2,*} and Rajesh KUMAR³

¹Department of Mathematics, Faculty of Science, Zagazig University, Egypt

²Department of Computer Science, Faculty of Science, Shaqra University, Saudi Arabia

³Department of Electrical Engineering, Malaviya National Institute of Technology, Jaipur, India

(* Corresponding author; e-mail: rmfarouk1@yahoo.com)

Received: 20 April 2012, Revised: 28 July 2012, Accepted: 9 December 2012

Abstract

In this paper, we present the elastic bunch graph matching as a new approach for iris recognition. The task is difficult because of iris variation in terms of position, size, and partial occlusion. We have used the circular Hough transform to determine the iris boundaries. Individual segmented irises are represented as labeled graphs. We have combined a representative set of individual model graphs into a stack like structure called an iris bunch graph (IBG). Finally, a bunch graph similarity function is proposed to compare a test graph with the IBG. Recognition results are given for galleries of irises from CASIA version and UBIRIS databases. The numerical results show that, the elastic bunch graph matching is an effective technique for iris matching. We also compare our results with previous results and find that, the elastic bunch graph matching is an effective matching performance.

Keywords: Iris recognition, iris localization and segmentation, bunch graph matching, feature extraction, Gabor wavelets

Introduction

Whenever people access an ATM, log on to computers, use credit cards, pass through airport security, or enter high-security areas, they need to verify their identities. People typically use user names, passwords, and identification cards to prove that they are who they claim to be. However, passwords can be forgotten, and identification cards can be lost or stolen. The recognition of persons has always been an attractive goal in computer vision. As in all pattern recognition or classification problems, the key issue is the relationship between inter-class and intra-class variability: objects can be reliably classified only if the variability among different instances of a given class is less than the variation between different classes. Thus, there is tremendous interest in improved methods of reliable and secure identification of people. Biometrics techniques are inherently a more reliable and capable technique to determine a person's identity by his or her own physiological or behavioral characteristics. The

features used for personal identification by current biometric applications include facial features, fingerprints, iris, palm-prints, retina, voice, handwritten signature, DNA and gait [1,2].

The developments in science and technology have made it possible to use biometrics in applications where it is required to establish or confirm the identity of individuals. Applications such as passenger control in airports, access control in restricted areas, border control, database access and financial services are some of the examples where biometric technology has been applied for more reliable identification and verification.

The human iris is an annular part between the pupil and sclera and its complex pattern contains many distinctive features such as arching ligaments, furrows, ridges, crypts, corona, and freckles. At the same time the iris is protected from the external environment behind the cornea and the eyelids. The reader's two eyes, directed at this

page, have identical genetics; they will likely have the same color and may well show some large scale pattern similarities; nevertheless, they have quite different iris pattern details. Elastic graph matching is a well-known approach in the face recognition area, and it is discussed for iris recognition in [3]. Elastic bunch graph matching is an extension approach of elastic graph matching for face recognition [4]. In this work, we present an elastic bunch graph matching as a new approach for iris recognition.

Related work

In an iris recognition system, iris localization is an essential step that spends nearly more than half of the entire processing time. The correctness of iris segmentation is required for the latter processes such as normalization, feature extraction and pattern matching. For those reasons, to improve the speed and accuracy of iris location becomes non-trivial. Daugman introduced the first use of integro-differential operator for localizing iris regions along with removing possible eyelid noises [5]. Some methods made certain improvement based on the Daugman's method [6]. The iris recognition becomes a promising topic of biometrics and gets more and more attention [7,8]. But it is still not in everyday use because of the complexity of the system.

Recently study presented improvements of these methods or new approaches for iris segmentation, pupil localization, and non-ideal iris image matching. At this time, essentially all of the large scale implementations of iris recognition are based on the Daugman iris recognition algorithms. The difference between a pair of iris codes was measured by their Hamming distance [9]. Wildes [10], combined the method of edge detection with the Hough transform for iris location. However, the parameters need to be precisely set and lengthy location time is required. Boles and Boashash [11] calculated zero-crossing representation of one-dimensional wavelet transformations at various resolution levels of a concentric circle on an iris image to characterize the texture of the iris. Iris matching was based on two dissimilarity functions. Huang *et al.* [12,13] decomposed an iris image into four levels using a 2-D Haar wavelet transform and quantized the fourth-level high-frequency information to form an 87-bit code. In another approach by Ma *et al.* [14] even symmetry Gabor filters are used to capture local texture

information of the iris, which are used to construct a fixed length feature vector.

In the last year only, the iris has been the attention of many researchers and different ideas have been formulated and published. For example, Abhyankara and Schuckers [15] presented a bi-orthogonal wavelet based iris recognition system, which modified and demonstrated to perform off-angle iris recognition. An efficient and robust segmentation of noisy iris images for non-cooperative iris recognition is described by Tan *et al.* [16]. Iris image segmentation and sub-optimal images is discussed by Matey *et al.* [17]. Comparison and combination of iris matchers for reliable personal authentication are introduced by Kumar and Passi [18]. Noisy iris segmentation, with boundary regularization and reflections removal, is discussed by Labati and Scott [19]. A multi-dimensional neural network iris recognition system is presented by Farouk *et al.* [20].

Hugo and Gil [21], presented a method for the recognition of degraded iris images acquired at visible wavelengths. The recognition scheme is based on the definition of homogeneous regions inside the iris. The description of each region is made by both shape and color MPEG 7 descriptors. Minimal levels of linear correlation between the proposed method and state-of-the-art techniques were observed. Iris representation based on binary features of the multi-scale Taylor expansion is discussed in [22]. The relationship between the accuracy of the iris segmentation process and the error rate of three typical iris recognition methods is presented in [23]. A non-ideal iris image segmentation approach based on graph cut is presented that uses both the appearance and eye geometry information [24]. The changes in iris texture with time, like disease and medication are discussed in [25]. In view of the limitation of poor direction selectivity about the 2-D wavelet transform and the problem of redundancy on contour let transform, an iris texture feature extraction method based on wavelet-based contourlets transform (WBCT) for obtaining high quality features is proposed in [26]. The construction of the histogram of a monochrome image, using different smoothing filters according to different monochrome location of the boundary area in an iris image, analyzing the regional value of the iris boundary and accomplishing the localization depending on the polling system by computing the possible

boundary points is proposed in [27]. A feature correlation evaluation approach for the iris image quality measure, which can discriminate the artificial patterns from the natural iris patterns and can also measure iris image quality for uncompressed images, is proposed in [28]. An effective approach for iris recognition using phase-based image matching is discussed in [29].

Outline

In this paper, we first present the circular Hough transform for iris preprocessing (segmentation step) which is a crucial step to the success of any iris recognition system. Once the iris region is successfully segmented from an eye image, the next stage is to present each iris image as a graph of a fixed iris region so that it has fixed dimensions in order to allow comparisons, then we have combined a representative set of individual model graphs into a stack like structure called an iris bunch graph (IBG). Finally, a bunch graph similarity function is proposed to compare a test graph with the IBG.

Iris segmentation

It is the stage of locating the iris region in an eye image; where as mentioned the iris region is the annular part between pupil and sclera. The iris segmentation has been achieved by the following three main steps. The first step locates the center and radius of the iris in the input image by using the circular Hough transform. Then a set of points is taken as pupil initialization from the nearby points to the iris center. The last step locates the pupil boundary points by using the region-based active contours.

Hough transform

The Hough transform is a standard computer vision algorithm that can be used to determine the parameters of simple geometric objects, such as lines and circles, present in an image. The circular Hough transform can be employed to deduce the radius and center coordinates of the pupil and iris regions. For instance, recognition of a circle can be achieved by considering the strong edges in an image as the local patterns and searching for the maximum value of a circular Hough transform. An automatic segmentation algorithm based on the circular Hough transform is employed in the localization method, similar to Daugman's method, and also based on the first derivative of the image.

In the proposed method by Wildes, an edge map of the image is first obtained by thresholding the magnitude of the image intensity gradient:

$$|\nabla G(x, y) * I(x, y)|, \quad (1)$$

$$G(x, y) = \frac{1}{2\pi\sigma^2} \exp\left(-\frac{(x-x_0)^2 + (y-y_0)^2}{2\sigma^2}\right) \quad (2)$$

where $G(x, y)$ is a Gaussian smoothing function with scaling parameter σ to select the proper scale of edge analysis. Firstly, an edge map is generated by calculating the first derivatives of intensity values in an eye image and then thresholding the result. From the edge map, votes are cast in Hough space to maximize the defined Hough transform for the desired contour. The obtained edge points are considered the parameters of circles passing through each edge points as $(x_i, y_i), i = 1, 2, \dots, n$. These parameters are the center coordinates x_c and, and the radius r , which are able to define any circle according to the equation:

$$x_c^2 + y_c^2 = r^2 \quad (3)$$

A Hough transform can be written as:

$$H(x_c, y_c, r) = \sum_{i=1}^n h(x_i, y_i, x_c, y_c, r), \quad (4)$$

$$h(x_i, y_i, x_c, y_c, r) = \begin{cases} 1 & \text{if } g(x_i, y_i, x_c, y_c, r) = 0 \\ 0 & \text{otherwise} \end{cases} \quad (5)$$

where

$g(x_i, y_i, x_c, y_c, r) = (x_i - x_c)^2 + (y_i - y_c)^2 - r^2$ is a parametric function. The edge points that are located over the circle result in a zero value of the function g . The value of g is then transformed to 1 by the h function, which represents the local pattern of the contour. The local patterns are then used in a voting procedure using the Hough

transform, H in order to locate the proper pupil and limbus boundaries **Figure 1**. In order to detect the limbus, only vertical edge information is used. The upper and lower parts, which have the horizontal

edge information, are usually covered by the two eyelids. The horizontal edge information is used for detecting the upper and lower eyelids, which are modeled as parabolic arcs.

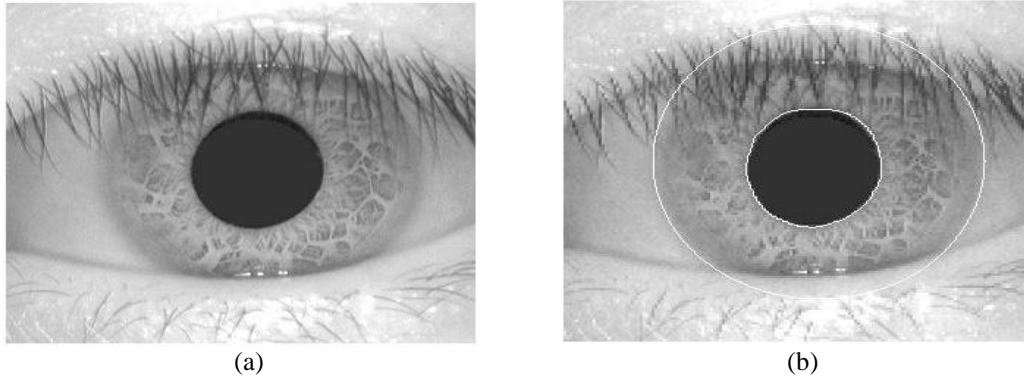


Figure 1 Segmentation of a sub-optimal iris image: (a) the original iris image, (b) the final segmentation.

Detecting eyelids, Eyelashes and noise regions

The eyelids are detected by first fitting a line to the upper and lower eyelid using the linear Hough transform. A horizontal line is then drawn which intersects with the first line at the iris edge that is closest to the pupil. A second horizontal line allows the maximum isolation of eyelid regions. Detecting eyelashes requires a proper choice of features and classification procedure due to the complexity and randomness of the patterns. The proposed eyelash detection by Daugman, considers eyelashes as two groups of separable eyelashes, which are isolated in the image, and multiple eyelashes, which are bunched together and overlap in the eye and applies two different feature extraction methods to detect eyelashes. Separable eyelashes are detected using a 1-D Gabor filter,

since the convolution of a separable eyelash with the Gaussian smoothing function results in a low output value. Thus, if a resultant point is smaller than a threshold, it is noted that this point belongs to an eyelash. Multiple eyelashes are detected using the variance of intensity. If the variance of intensity values in a small window is lower than a threshold, the center of the window is considered as a point in an eyelash. The two features combined with a connectivity criterion would lead to the decision of the presence of eyelashes. In addition, an eyelash detection method is also proposed by Huang *et al.* [13] that uses the edge information obtained by phase congruency of a bank of Log-Gabor filters. The edge information is also infused with the region information to localize the noise regions **Figure 2**.

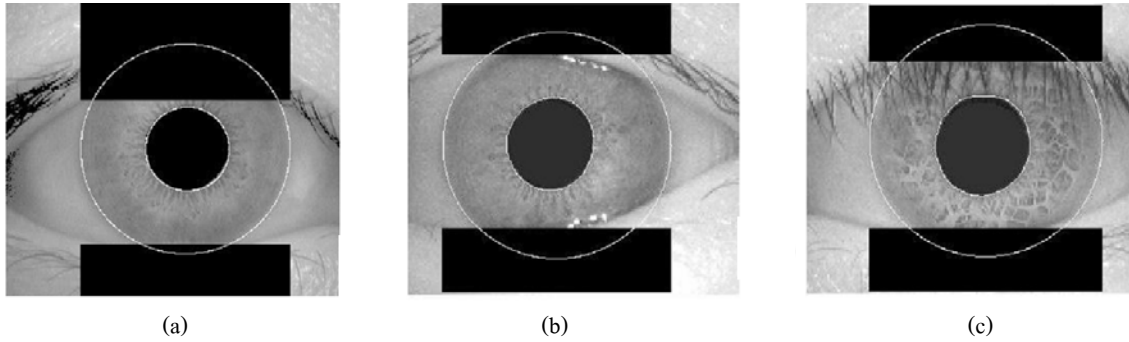


Figure 2 The iris localization, where black regions denote detected eyelids and eyelashes regions.

Kong and Zhang [30] presented an approach intended to deal with the presence of eyelashes and specular reflections. Eyelashes are dealt with as “separable” and “mixed.” Separable eyelashes can be distinguished against the texture of the iris, whereas mixed eyelashes present a larger region of occlusion.

Gabor wavelet

Gabor wavelets were introduced into image analysis due to their biological relevance and computational properties [31]. The Gabor wavelets, whose kernels are similar to the 2D receptive field profiles of the mammalian cortical simple cells, exhibit desirable characteristics of spatial locality and orientation selectivity, and are optimally localized in the space and frequency domains. The Gabor wavelets (kernels, filters) can be defined as follows:

$$\psi_{\mu,\nu}(\vec{x}) = \frac{\|k_{\mu,\nu}\|^2}{\sigma^2} \exp\left[-\frac{\|k_{\mu,\nu}\|^2 \|\vec{x}\|^2}{\sigma^2}\right] \left[\exp^{i\vec{k}_{\mu,\nu}\vec{x}} - \exp^{-\frac{\sigma^2}{2}} \right] \quad (6)$$

Where μ and ν define the orientation and scale of the Gabor kernels, $\| \cdot \|$ denotes the norm operator, and the wave vector is defined as follows:

$$\vec{k}_{\mu,\nu} = k_\nu \exp^{i\varphi_\mu} \quad (7)$$

Where $k_\nu = \frac{k_{\max}}{f^\nu}$ and $\varphi_\mu = \frac{\mu\pi}{8}$. k_{\max} is the maximum frequency, and f is the spacing factor between kernels in the frequency domain [21].

The Gabor kernels in Eq. (6) are all self-similar since they can be generated from one filter, the mother wavelet, by scaling and rotating via the wave vector $\vec{k}_{\mu,\nu}$. Each kernel is a product of a Gaussian envelope and a complex plane wave, while the first term in the square brackets in Eq. (6) determines the oscillatory part of the kernel and

the second term compensates for the DC value. The effect of the DC term becomes negligible when the parameter σ , which determines the ratio of the Gaussian window width to wavelength, has sufficiently large values. In most cases one would use Gabor wavelets of five different scales, $\nu = 0,1,2,3,4$, and eight orientations, $\mu = 0,1,2,\dots,7$ [35]. **Figure 3** shows the real part of the Gabor kernels at five scales and eight orientations and their magnitude, with the following parameters: $\sigma = 2\pi$, $k_{\max} = \frac{\pi}{2}$ and $f = \sqrt{2}$. The kernels exhibit desirable characteristics of spatial frequency, spatial locality, and orientation selectivity.

Jet feature representation

The Gabor wavelet representation of an iris image is the convolution of the iris image with a family of Gabor kernels as defined by Eq. (6). Let $I(x)$ be the gray level distribution of an iris image, the convolution of iris image $I(x)$ and Gabor kernels $\psi_{\mu,v}$ around a given pixel \vec{x} defined as follows:

$$Y_{\mu,v}(\vec{x}) = (\psi_{\mu,v} * I)(\vec{x}) \quad (8)$$

Where $*$ denotes the convolution operator, and $Y(\vec{x})$ is the convolution result corresponding to the Gabor kernel at orientation μ and scale v . Therefore, the set $\{Y_{\mu,v} : \mu = 0, 1, \dots, 7, v = 0, 1, 2, 3, 4\}$ forms the Gabor wavelet representation of the iris image $I(x)$. Applying the convolution theorem, we can derive each $Y_{\mu,v}$ from Eq. (8) via the Fast Fourier Transform (FFT):

$$\mathfrak{F}\{Y_{\mu,v}(\vec{x})\} = \mathfrak{F}\{\psi_{\mu,v}\}\mathfrak{F}\{I(\vec{x})\} \quad (9)$$

and

$$Y_{\mu,v}(\vec{x}) = \mathfrak{F}^{-1}\{\mathfrak{F}\{\psi_{\mu,v}\}\mathfrak{F}^{-1}\{\mathfrak{F}\{I(\vec{x})\}\}\} \quad (10)$$

Where \mathfrak{F} and \mathfrak{F}^{-1} denote the Fourier and inverse Fourier transform, respectively.

Figure 3 shows the Gabor wavelet representation (the real part, imaginary part and the magnitude) of an iris image. These representation results display scale, locality, and orientation properties corresponding to those displayed by the Gabor wavelets. To encompass different spatial frequencies (scales), spatial localities, and orientation selectivity, we concatenate all these representation results and derive an augmented feature vector (jet) Γ . A jet Γ is defined as the set $\{Y_{\mu,v} : \mu = 0, 1, \dots, 7, v = 0, 1, 2, 3, 4\}$ of 40 complex coefficients obtained for one iris image point. It can be written as

$$\Gamma(\vec{x}_0) = \{Y_{\mu,v} : \mu = 0, 1, \dots, 7, v = 0, 1, 2, 3, 4\} \quad (11)$$

This array of numbers is used as a feature vector to characterize the iris image blob at location \vec{x}_0 .

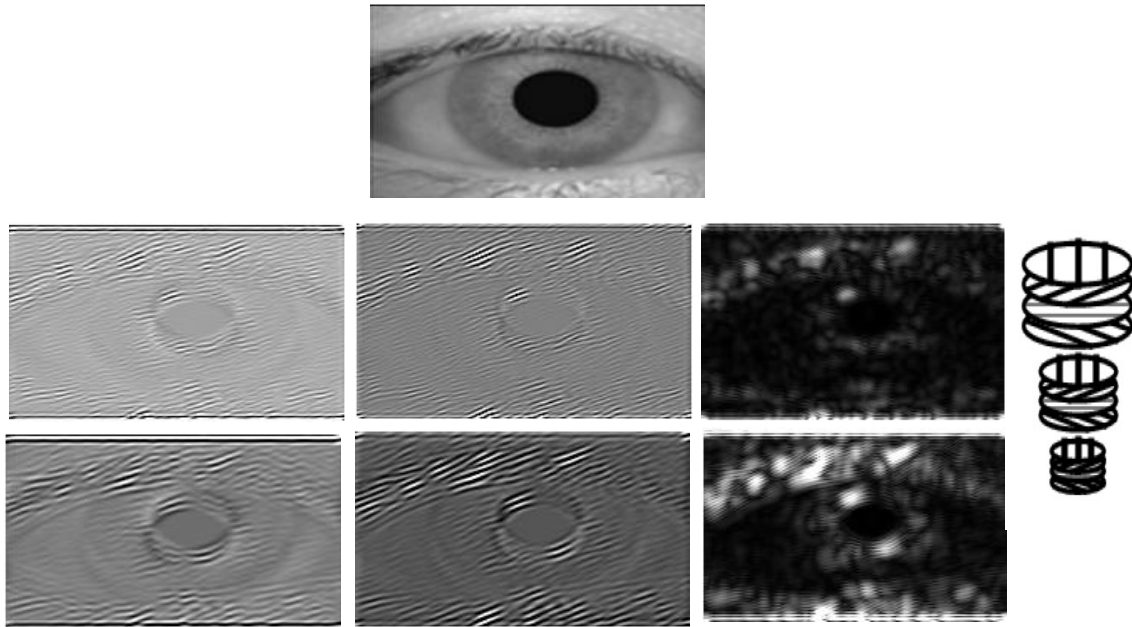


Figure 3 Original image at the top, the first column on the left shows the real part of the complex wavelet transform Eq. (9), the second column on the right shows imaginary part and the third column shows the absolute value for two different scales, on the right is the jet extracted at a given point \vec{x}_0 .

Comparing jets

After we have represented each iris image with Gabor wavelets, we compute the similarity between each iris blob (Gabor jet). For two jets Γ and Γ' a similarity value $S(\Gamma, \Gamma')$ is defined as the normalized scalar product (considering jets simply as vectors) as defined in Eq. (12).

$$S(\Gamma, \Gamma') = \frac{\sum_j a_j a'_j}{\sqrt{\sum_j a_j^2 \sum_j a_j'^2}} \tag{12}$$

This is used when comparing jets taken from two iris images or from an iris image and an iris model graph. Using phase has two potential advantages. Firstly, phase information is required to discriminate between patterns with similar magnitudes, should they occur, and secondly, since phase varies so quickly with location, it provides a means for accurate jet localization in an iris image. Assuming that two jets Γ and Γ' refer to iris locations with small relative displacement \vec{d} , the

phase shifts can be approximately compensated for by the terms $\vec{d}\vec{k}$, leading to a phase-sensitive similarity function

$$S_{ph}(\Gamma, \Gamma') = \frac{\sum_j a_j a'_j \cos(\varphi_j - \varphi'_j - \vec{d}\vec{k})}{\sqrt{\sum_j a_j^2 \sum_j a_j'^2}} \tag{13}$$

to compute it, the displacement \vec{d} has to be estimated. This can be done by maximizing S_{ph} in its Taylor expansion, as explained in [32]. It is actually a great advantage of this second similarity function that it yields this displacement information.

Bunch jet extraction

To extract a bunch jet β at a point \vec{x} from our database, we have combined a representative set of individual jet Γ at the same point of the iris image into a stack-like structure, called bunch jet β at the point \vec{x} , **Figure 4**.

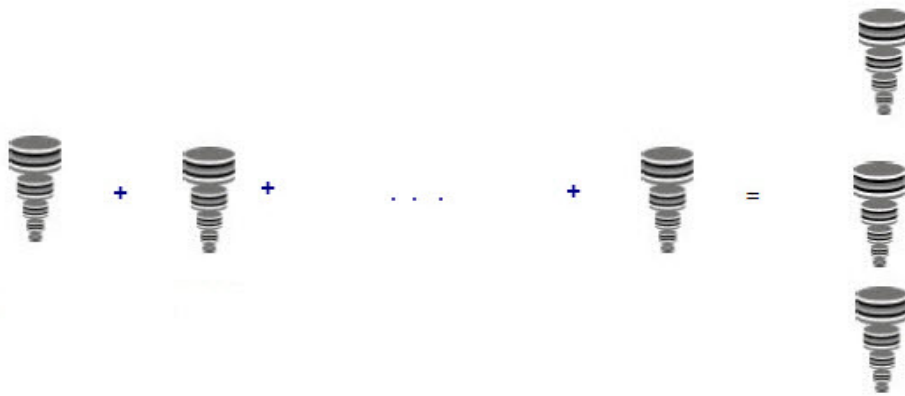


Figure 4 Shows the extraction of bunch graph jet.

Iris graph formulation

During the last decade, the use of graph-based object representation has drastically increased. As a matter of fact, object representation by means of graphs has a number of advantages over feature vectors. As a consequence, methods to compare graphs have become of first interest. In this paper, a graph matching method and a distance between attributing graphs are defined. Each iris image is represented as a labeled graph. Nodes are labeled with jets; edges are labeled with distance vectors in **Figure 5**. In the work reported here, we have treated the edge labels implicitly by just storing the positions of nodes as two-dimensional coordinates and creating

distance information from coordinates whenever needed. Thus the natural substrate to represent an image graph is based on a jet and a pixel index pair. Permanently stored model graphs are formed from sparse subsets of pixels forming a semi-circular graph.

In our system we describe the relationship of the model domain to the image domain with the help of a few binary variables that decide on the recognition status of a model and the visibility or occlusion (eyelashes and eyelids regions see **Figure 2**) of its individual nodes, plus a single position vector for the placement of the model graph in the image. These variables will be introduced in the next section.

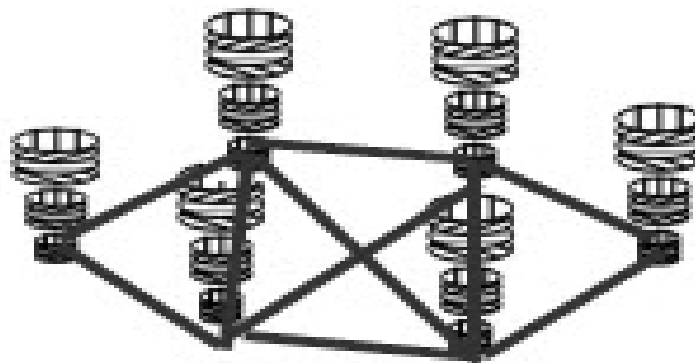


Figure 5 Diagram showing the iris graph representation; some edges are invisible for simplicity.

Iris bunch graph formulation

A general representation of the individual iris should cover a wide range of possible variations in the appearance of irises, such as differently shaped eyes, light reflection or light spots and partial occlusion [31]. It is obvious that it would be too expensive to cover each feature combination by a

separate graph. We instead combine a representative set of individual model graphs into a stack-like structure, called an iris bunch graph **Figure 6**. Each model graph has the same grid structure and the same number of nodes refers to identical iris points.



Figure 6 Representation of the iris bunch graph formulation.

Elastic bunch graph matching

To compute the graph similarity between an iris image graph and the IBG, it depends on the jet similarities and the distortion of the iris image grid relative to the IBG grid. For an iris image graph G^I with nodes $n = 1, \dots, N$ and edges $e = 1, \dots, E$ and an iris bunch graph B of $m = 1, \dots, M$ model graphs. The similarity is defined as Eq. (14):

$$S_B(G^I, B) = \frac{1}{N} \sum_n \max_m (S(\Gamma_n^I, \Gamma_n^{Bm})) \quad (14)$$

where Γ_n the image jet is extracted at node n and Γ_n^{Bm} is the corresponding jet at node n of m graph in the bunch graph. The result of matching is illustrated in **Figure 7**.

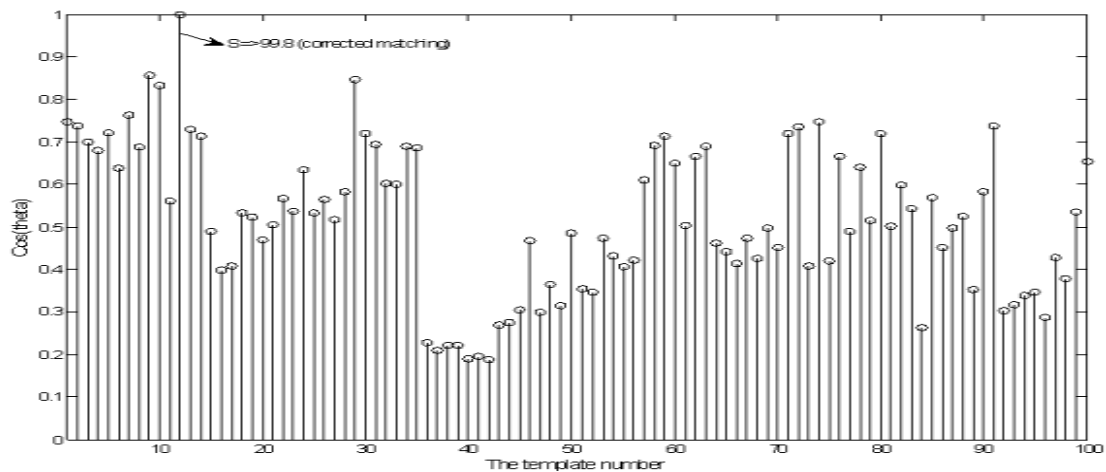


Figure 7 The matching of the template graph of an image in CASIA against 100 stored bunch graph, where $S(\Gamma_i^I, \Gamma_i^M)$ is the similarity between the two graphs.

Algorithm of IBG

1. Estimate location of features or nodes
 $n = 1, \dots, N$

2. For each point x_0 :

1. Calculate convolutions with all wavelets

$$\Gamma(\bar{x}_0) = \{Y_{\mu,\nu} : \mu = 0, 1, \dots, 7, \nu = 0, 1, 2, 3, 4\}$$

2. Find the displacement (it can be used for detection)

3. Correct the Jet for the new location

3. Feature vectors comparison:

1. For $n = 1, \dots, N$ computes, $S(\Gamma, \Gamma')$

2. To compute the matching of the model G^I with IBG

For all graphs $m = 1, \dots, M$

$$S_B(G^I, B)$$

3. Maximum similarity

$$\frac{1}{N} \sum_n \max_m (S(\Gamma_n^I, \Gamma_n^{Bm}))$$

Iris database

In this paper we have used two freely and large publicly available databases of iris, CASIA and UBIRIS [33,34]. The iris database of CASIA (CASIA-Iris V. 3-Interval) is a free to use open iris database and we only use a subset for performance evaluation, CASIA-Iris V. The 3-Interval database includes about 1992 iris images captured from 249 different persons (hence, 249 different classes) with eight images captured for each person. Each iris image has a resolution of 320×280 in 8-bit gray level. Four images of each class are selected randomly to constitute the training set and the remaining images are the test set. In the first processing stage, we checked the segmentation accuracy of the iris boundaries subjectively and obtained an accuracy rate of 93:9 % (89 images are not used), as shown in **Table 1**, which shows different causes resulting in the failure of iris locating. Therefore, there are 981 images for training and 915 images for testing.

Table 1 Failure analysis of locating iris for different causes.

Cause of failure	Number of images	
	CASIA	UBIRIS
Occlusion by eyelids	36	6
Inappropriate eye positioning	21	13
Occlusion by eyelash	23	11
Noises within iris	6	4
Total	86	34

The UBIRIS iris database is composed of 1205 images collected from 241 persons (five images for each eye). Each iris image size has a resolution of 200×150 in JPEG format. For each iris class, we choose three samples at random for training and the remaining ones as test samples.

After preprocessing, the obtained accuracy rate is 97:17 % (34 images are not used), as shown in **Table 1**. Therefore, there are 723 images for training and 448 images for testing. The matching process is displayed in **Figure 8**.

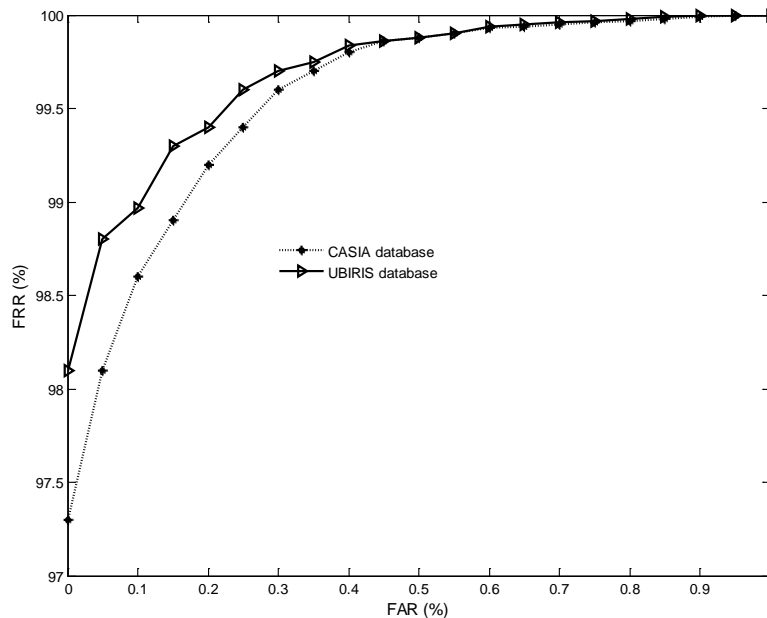


Figure 8 The ROC curves of the elastic graph matching with CASIA and UBIRIS databases.

Results

To evaluate the effectiveness and the performance of the proposed method for iris recognition, we have used the CASIA version 1 [33] and UBIRIS databases [34] as the test and train dataset. The experiments are conducted in two modes: verification and identification. In the verification mode, the Receiver Operating Characteristic (ROC) curve depicts the relationship of False Accept Rate (FAR) versus False Reject Rate (FRR). The area under the ROC curve (denoted as AZ) reflects how well the intra-class and extra-class distributions can be distinguished and the ranges are from 0.5 to 1. For an ideal ROC curve, the value of AZ should be 1. It denotes that the intra and extra-class are inseparable while the AZ value is equal to 0.5. Hence, the ROC curve is suitable for measuring the accuracy of the matching process and showing the achieved

performance of a recognition algorithm. FAR is the probability of accepting an imposter as an authorized subject and FRR is the probability of a genuine authorized subject that is rejected as being an imposter. In the recognition mode, the Correct Recognition Rate (CRR) is adopted to assess the efficacy of the algorithm, as shown in **Table 2**.

To assess the accuracy of the proposed algorithm, each test iris image in the database is individually matched to all the other iris images in the trained database. In the UBIRIS database, the total number of comparisons is 324351 where the numbers of intra-class and extra-class comparisons are 1792 and 322559 respectively. The EGM was tested using 996 and 723 iris images from the CASIA and UBIRIS database respectively. The ROC curve, **Figure 9** for the False Match Rate (FMR) and False Non-Match Rate (FNMR) are

estimated. The EBG was found to give good correct recognition rates compared to other matching methods as shown in **Table 2**. The result of matching is illustrated in **Figure 9**.

Table 2 The correct recognition rates achieved by four matching measures using the CASIA and UBIRIS database.

Matching measure	Correct recognition rate (CRR) %
Elastic Graph Match Farouk, 2011	98.5
Proposed EBM	98.8
Fourier-wavelet feature, Huang, 2005	98.4
Gaussian Hermit moments, Ma 2004	98.1

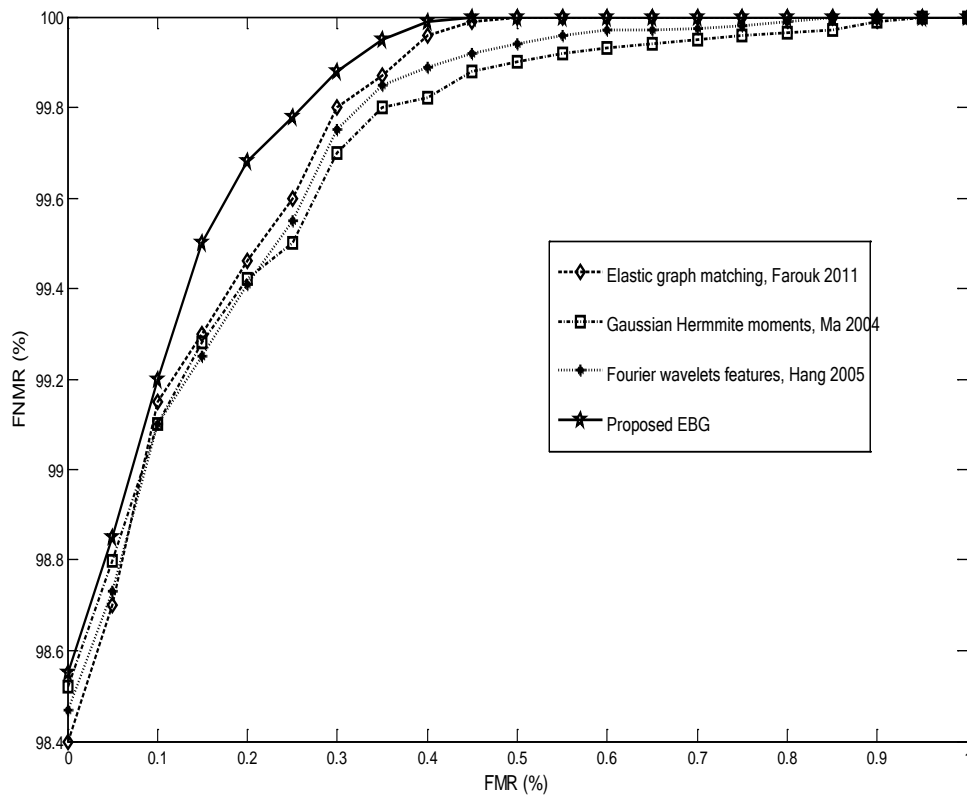


Figure 9 The obtained ROC curves after applying different methods on CASIA database.

Conclusions

Here we have presented a new and effective approach for iris recognition which operates using Elastic Bunch Graph Matching (EBGM). Also, we have found that the system depends strongly on the iris boundary. Experimental results have shown that ignoring the boundary effect still can indicate eminent performance for iris recognition. All recognition rates are more than 90 %. Therefore, the EBGM method has been demonstrated to be promising for iris recognition and is suitable for the matching process. In future work, we will improve the processing method for iris templates to reduce the influence of light, eyelids, and eyelashes. Also we will try to apply this approach to non-ideal iris images.

Acknowledgements

The authors would like to thank the associate editor and the anonymous reviewers for their constructive comments. The author also would like to thank Prof. Dr. Christopher von der Malsburg and all members of FLAVOR for giving him the opportunity to learn the EBM technique during PhD studies in Germany.

References

- [1] KW Boweyer, K Hollingsworth and JF Patrick. Image understanding for iris biometrics: A survey. *Comput. Vis. Image Understand.* 2008; **110**, 281-307.
- [2] N Duta. A survey of biometric technology based on hand shape. *Pattern Recognit.* 2009; **42**, 2797-806.
- [3] L Wiskott, JM Fellows, N Kruege and C Malsburg. Face recognition by elastic bunch graph matching. *IEEE Trans. Pattern Anal. Mach. Intell.* 1997; **19**, 775-9.
- [4] RM Farouk. Iris recognition based on elastic graph matching and Gabor wavelet. *Comput. Vis. Image Understand.* 2011; **115**, 1239-44.
- [5] J Daugman. High confidence visual recognition of persons by a test of statistical independence. *IEEE Trans. Pattern Anal. Mach. Intell.* 1993; **15**, 1148-61.
- [6] J Daugman. Demodulation by complex-valued wavelets for stochastic pattern recognition. *Int. J. Wavelets, Multiresolution Inform. Process.* 2003; **1**, 1-17.
- [7] J Daugman. Statistical richness of visual phase information: update on recognizing persons by Iris patterns. *Int. J. Comput. Vis.* 2001; **45**, 25-38.
- [8] J Daugman. How Iris recognition works. *IEEE Transactions on Circuits and Systems for Video Technology* 2004; **14**, 21-30.
- [9] J Daugman. The importance of being random: statistical principles of Iris recognition. *Pattern Recognit.* 2003; **36**, 279-91.
- [10] RP Wildes. Iris recognition: An emerging biometric technology. *Proc. IEEE* 1997; **85**, 1348-63.
- [11] W Boles and B Boashash. A human identification technique using images of the Iris and Wavelet transform. *IEEE Trans. Signal Process.* 1998; **46**, 1185-8.
- [12] PS Huang, CS Chiang and JR Liang. Iris recognition using Fourier-wavelet features. *Lect. Notes Comput. Sci.* 2005; **3546**, 14-22.
- [13] J Huang, Y Wang, T Tan and J Cui. A new iris segmentation method for recognition. In: *Proceedings of the 17th International Conference on Pattern Recognition*, Cambridge, UK. 2004, p. 554-7.
- [14] L Ma, T Tan, Y Wang and D Zhang. Local intensity variation analysis for iris recognition. *Pattern Recognit.* 2004; **37**, 1287-98.
- [15] A Abhyankara and S Schuckers. A novel biorthogonal wavelet network system for off-angle iris recognition. *Pattern Recognit.* 2010; **43**, 987-1007.
- [16] T Tan, Z He and Z Sun. Efficient and robust segmentation of noisy iris images for non-cooperative iris recognition. *Image Vis. Comput.* 2010; **28**, 223-30.
- [17] J Matey, R Broussard and RL Kennell. Iris image segmentation and sub-optimal images. *Image Vis. Comput.* 2010; **28**, 215-22.
- [18] A Kumar and A Passi. Comparison and combination of iris matchers for reliable personal authentication. *Pattern Recognit.* 2010; **43**, 1016-26.
- [19] RD Labati and F Scott. Noisy iris segmentation with boundary regularization and reflections removal. *Image Vis. Comput.* 2010; **28**, 270-7.
- [20] RM Farouk, R Kumar and KA Raid. Iris matching using multi-dimensional artificial

- neural network. *IET Comput. Vis.* 2011; **5**, 178-84.
- [21] P Hugo and S Gil. Fusing color and shape descriptors in the recognition of degraded iris images acquired visible wavelength. *Comput. Vis. Image Understand.* 2012; **116**, 167-78.
- [22] B Algrids, K Justas and K Volker. Iris recognition by fusing different representations of multi-scale Taylor expansion. *Comput. Vis. Image Understand.* 2011; **115**, 804-16.
- [23] H Proença and LA Alexandre. Iris recognition: Analysis of the error rates regarding the accuracy of the segmentation stage. *Image Vis. Comput.* 2010; **28**, 202-6.
- [24] S Pundlik, D Woodard and S Birchfield. Iris segmentation in non-ideal images using graph cuts. *Image Vis. Comput.* 2010; **28**, 1671-81.
- [25] DM Rankin, BW Scotney, PJ Morrow and BK Pierscionek. Iris recognition failure over time: The effects of texture. *Pattern Recognit.* 2012; **45**, 145-50.
- [26] Z Luo. Iris feature extraction and recognition based on wavelet based contourlet transform. *Procedia Eng.* 2012; **29**, 3578-82.
- [27] ZX Ye and YZ Zhuang. A new and fast algorithm of Iris location. *Comput. Eng. Appl.* 2003; **30**, 54-6.
- [28] Y Du, C Belcher, Z Zhou and R Ives. Feature correlation evaluation approach for iris feature quality measure. *Signal Process.* 2010; **90**, 1176-87.
- [29] K Miyazawa, K Ito, T Aoki, K Kobayashi and H Nakajima. An effective approach for iris recognition using phase-based image matching. *IEEE Trans. Pattern Anal. Mach. Intell.* 2008; **30**, 1741-56.
- [30] W Kong and D Zhang. Detecting eyelash and reflection for accurate iris segmentation. *Int. J. Pattern Recognit. Artif. Intell.* 2003; **17**, 1025-34.
- [31] JG Daugman. Complete discrete 2-d Gabor transforms by neural networks for image analysis and compression. *IEEE Trans. Pattern Anal. Mach. Intell.* 1988; **36**, 1169-79.
- [32] L Wiskott, JM Fellous, N Kruger and C von der Malsburg. Face recognition by elastic bunch graph matching. *IEEE Trans. Pattern Anal. Mach. Intell.* 1997; **19**, 775-9.
- [33] CASIA Iris Image Database, Available from: <http://www.sinobiometrics.com>.
- [34] HL Proenca and A Alexandre. UBIRIS: A noisy iris image database, Available from: <http://iris.di.ubi.pt>.